Received: 29 April 2016 | Accepted: 11 August 2016

DOI: 10.1111/jace.14488

ORIGINAL ARTICLE

Journal of the American Ceramic Society

The temperature dependence of the relative grain-boundary energy of yttria-doped alumina

Madeleine N. Kelly | Stephanie A. Bojarski | Gregory S. Rohrer

Department of Materials Science and Engineering, Carnegie Mellon University, Pittsburgh, Pennsylvania

Correspondence
Gregory S. Rohrer, Department of Materials Science and Engineering, Carnegie Mellon University, Pittsburgh, PA.
Email: gr20@andrew.cmu.edu

Abstract

Atomic force microscopy was used to measure the dimensions of grain-boundary thermal grooves on the surfaces of Al_2O_3, 100 ppm Y-doped Al_2O_3, and 500 ppm Y-doped Al_2O_3 ceramics heated at temperatures between 1350°C and 1650°C. The measurements were used to estimate the relative grain-boundary energies as a function of temperature. The relative grain-boundary energies of Al_2O_3 decrease slightly with increased temperature. When the doped samples were heated, there was an overall increase in the grain-boundary energy, attributed to a reduction in the grain boundary excess at higher temperature. The overall trend of increasing grain-boundary energy was interrupted by abrupt reductions in grain-boundary energy between 1450°C and 1550°C. In the same temperature range, there is an abrupt increase in the grain-boundary mobility that is associated with a complexion transition. When the 100 ppm Y-doped sample was cooled, there was a corresponding increase in the relative grain-boundary energy at the same complexion transition temperature, indicating that the transition is reversible.

KEYWORDS

alumina, grain boundaries, grain growth, microstructure

1 | INTRODUCTION

In most models for microstructure evolution, the grain-boundary energy is taken to be a constant. However, it is known from both experiments[1] and simulations[2,3] that the grain-boundary energy can change with temperature and these changes have the potential to affect microstructure evolution. For example, changes in the grain-boundary energy with temperature have been implicated in anti-thermal grain growth phenomena in $SrTiO_3$.[4,5] Abrupt changes in the grain-boundary energy have also been linked to complexion transitions and abnormal grain growth.[6,7] However, there is very little available data on the temperature dependence of the grain-boundary energy. The only previous study we are aware of, interpreted from grain-boundary diffusion measurements made 35 year ago, indicates that the grain-boundary energy of NiO increases by 14% when the temperature is increased by 600°C.[1,8] Here, we experimentally examine the temperature dependence of the grain-boundary energy in 99.995% pure and Y-doped alumina.

The grain-boundary excess free energy varies with temperature and there are several factors that influence the variation. First, the free energy is expected to decrease with increasing temperature because of the entropic contribution. This has been observed in a number of pure materials.[1,9,10] In materials containing segregating impurities, the grain-boundary energy will be affected by changes in the grain-boundary composition. In most cases, the grain-boundary energy decreases with increases in the grain-boundary excess solute content. Because bulk solubility typically increases with temperature, solute from the intergranular regions can dissolve in the bulk as the temperature is increased, reducing the grain-boundary excess (desegregation). This will lead to an increase in the grain-boundary free energy with temperature. Desegregation influences the grain-boundary energy in a way opposite to entropy; past studies have shown that

changes from desegregation are usually more significant than those associated with entropy, so for impure materials, the grain-boundary energy usually increases with temperature.[1]

Entropy and desegregation both lead to continuous changes in the grain-boundary energy. One can imagine that if grain boundaries are supersaturated in solute and a second phase precipitates, the formation of a second phase would abruptly reduce the grain-boundary excess and increase the energy. In polycrystals where the solvent phase has already saturated the grain boundaries, any grain growth will lead to a reduction in the intergranular area, which could supersaturate the boundaries prior to the formation of a second phase. While boundary supersaturation followed by precipitation has been reported,[11] measurements of the grain-boundary energy during this series of transitions has not been reported.

An abrupt transition in grain-boundary energy might also occur if there is a transition in the structure and/or chemical composition of the grain boundary; this is referred to as a complexion transition.[12] The energy changes associated with transitions have been evaluated using measurements of the grain-boundary thermal groove geometry.[7,13,14] In this experiment, a microstructure is produced in which two grain-boundary complexions are expected to coexist, based on the presence of a bimodal grain size distribution. When the relative energies of the grain boundaries surrounding the very large grains are compared to those around the smallest grains, there is usually a significant difference. For example, in 100 ppm Y-doped alumina at 1400°C, the energies of the boundaries around large grains were 46% lower than around the small grains.[7]

The experiments comparing the relative energies of the different types of grain boundaries are interpreted with respect to the schematic in Figure 1. At low temperatures, all of the grain boundaries have a single stable complexion and a unimodal microstructure (Figure 1B). As temperature increases, one grain-boundary complexion might become more stable than another. If all of the boundaries transformed immediately to the lower energy complexion, then the rate of change of the grain-boundary energy with temperature will decrease at the temperature where the lines intersect, and the microstructure will remain unimodal. However, it is also possible that there is an activation barrier and the system must be superheated before the least stable boundaries transform. If so, the energy will follow the blue dashed line until the least stable boundaries transform to the lower energy complexion at the position of the vertical blue dashed line. If the high-temperature, low-energy complexion has a mobility advantage over the non-transformed boundaries, a microstructure with a bimodal grain size distribution will form (Figure 1C). The energy difference between the transformed grain boundaries around the large grains and the metastable boundaries around the small grains is labeled $\Delta\gamma$ in Figure 1A.

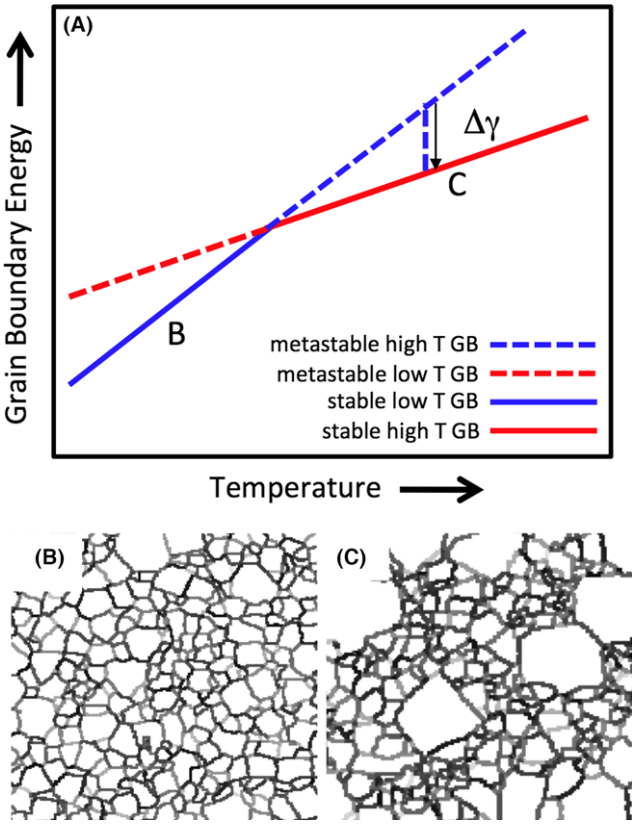

FIGURE 1 Schematic illustration of grain-boundary energies (A) and microstructure (B and C) in a material with two stable grain-boundary complexions that have very different grain-boundary mobilities. See text for explanation [Color figure can be viewed at wileyonlinelibrary.com]

The previous experiments evaluated the energy difference between the stable and metastable boundaries at a single temperature, but they do not tell us how the grain-boundary energy changes with temperature or determine the transition temperature. Therefore, the purpose of this paper is measure the temperature dependence of the relative grain-boundary energy in 99.995% pure, 100 ppm Y-doped, and 500 ppm Y-doped alumina. The relative grain-boundary energy is determined from AFM measurements of grain-boundary thermal grooves. The measurements are made as a function of increasing temperature for all three materials. Measurements were also made with decreasing temperature for the 100 ppm Y-doped alumina sample. The measurements show that the changes in the grain-boundary energy as a function of temperature are influenced by solute partitioning between the bulk and grain-boundary phase, and by complexion transitions.

2 | EXPERIMENTAL METHODS

Pure alumina ceramics were prepared from 99.995% pure alumina (Puratronic; Alfa Aesar, Ward Hill, MA). The

most concentrated impurities in the starting material were Na (10 ppm), Zr (9 ppm), Ca (4 ppm), Mg (3 ppm), and Fe (2 ppm). These concentrations, supplied by the manufacturer, are in weight fractions and were determined by inductively coupled plasma emission spectroscopy. Y-doped alumina (concentrations are Y per Al atoms) of 100 ppm and 500 ppm were prepared from the same alumina source, with appropriate amounts of added Y $(NO_3)_3{\cdot}6H_2O$ (Alfa Aesar). A micropipette was used to transfer appropriate amounts of Y (100 or 500 ppm) from a 0.05 $mol{\cdot}L^{-1}$ solution of $Y(NO_3)_3{\cdot}6H_2O$ and methanol to the 99.995% pure alumina, also suspended in methanol. This solution was mixed using a PTFE magnetic stir bar on a stirring hot plate. After evaporating the methanol from the suspension under a fume hood, the powders were dried at 100°C in air. After drying, the doped powders were placed in plastic bags and milled with a marble rolling pin to break up agglomerates. Consolidation of the powders was carried out by spark plasma sintering. About 10 g of powder were loaded in a graphite die. The ram was then inserted and the samples were spark plasma sintered (Thermal Technologies, LLC, Santa Clara, CA) using a ramp of 100°C per minute to 800°C for 45 minute at 10 MPa followed by another ramp cycle of 100°C per minute up to 1300°C for 30 minute at 50 MPa. The sample was then cooled to room temperature at a maximum rate of 150°C/min. The Archimedes method was used to measure the densities of the samples and they were found to be 96.7%, (99.995% pure), 98.5% (100 ppm Y), and 95.7% (500 ppm doped Y). Note that throughout this paper, we will refer to these samples as the 100 and 500 ppm samples, based on the synthesis conditions. The actual compositions after sintering were not determined.

Each of the samples was sectioned with a 12.7 mm diamond wafering blade mounted on a low-speed saw. These sectioned pieces were mounted in a cold-curing resin and polished with polycrystalline diamond, using a 0.05 μm polycrystalline diamond solution as the final step. After removing the samples from the mount, thermal grooving was carried out in a box furnace in air. The samples were placed in 98% pure alumina crucibles and heated at 10°C/min up to temperatures ranging from 1350°C to 1650°C and cooled back to room temperature at 20°C/min. The 500 and 100 ppm Y-doped alumina samples were thermally grooved for 3 and 5 hour, respectively, for the experiments with increasing temperature. The 99.995% pure samples were grooved for 3 hour. For the experiments where the grooves were measured with decreasing temperature, the samples were re-polished, to remove the grooves formed at high temperature, before grooving at the lower temperature. The average grain diameters of the samples after the lowest and highest temperature annealing were measured by the linear intercept method and the results are summarized in Table 1.

Atomic force microscopy (AFM) was used in contact mode to measure the groove geometry. Images were recorded with a 10 nm step size at a 1 Hz scan frequency using a Solver NEXT AFM (NT-MDT, Moscow, Russia). The pyramidal silicon nitride tips used for the measurements had a cone angle of 35°, a radius of less than 10 nm, a resonance frequency of 67 kHz, a force constant of 0.32 N/m, and a Cr/Au coating on the detector side (Pyrex Nitride Probes triangular shape, NanoWorld, Neuchâtel, Switzerland). The AFM images were taken at randomly selected locations on the surface, sampling all areas of the specimen.

The treatment of the AFM data followed a procedure described earlier.[15] Briefly, the images were processed to remove any overall slope. For each groove, three profiles were extracted, and the width (W) and depths (d) were measured automatically using a computer program (see Figure 2). Note that the groove shape is created by surface diffusion during the high-temperature anneal. Because of the rapidly decreasing diffusion rates on cooling, the high-temperature groove shape is locked in, even if the grain-boundary structure or composition changes at lower temperature. Because the grooves are usually asymmetric, the two sides are considered separately, as if they were two separate symmetric grooves. Knowing W and d, the ratio of the grain boundary to surface energy can be calculated using Equation (1).

$$\frac{\gamma_{gb}}{\gamma_s} = 2\sin\left(\tan^{-1}\left(m\left(\frac{d}{2W}\right)\right)\right) \quad (1)$$

where m is a constant equal to 4.73.[16] When using AFM to measure the relative grain-boundary energy, it is necessary

TABLE 1 Average grains sizes

Sample	Temperature (°C)	Average grain size (μm)
99.995% Pure	1450	2.4
99.995% Pure	1550	4.8
99.995% Pure	1650	10.2
100 ppm	1450	2.6
100 ppm	1500	2.9[a]
100 ppm	1525	3.4[a]
100 ppm	1550	5.2[a]
100 ppm	1650	8.8
500 ppm	1350	0.9
500 ppm	1400	1.4
500 ppm	1450	2.8
500 ppm	1500	2.4[a]
500 ppm	1550	4.0[a]
500 ppm	1600	6.9
500 ppm	1650	6.9

[a]Mean values of bimodal distributions.

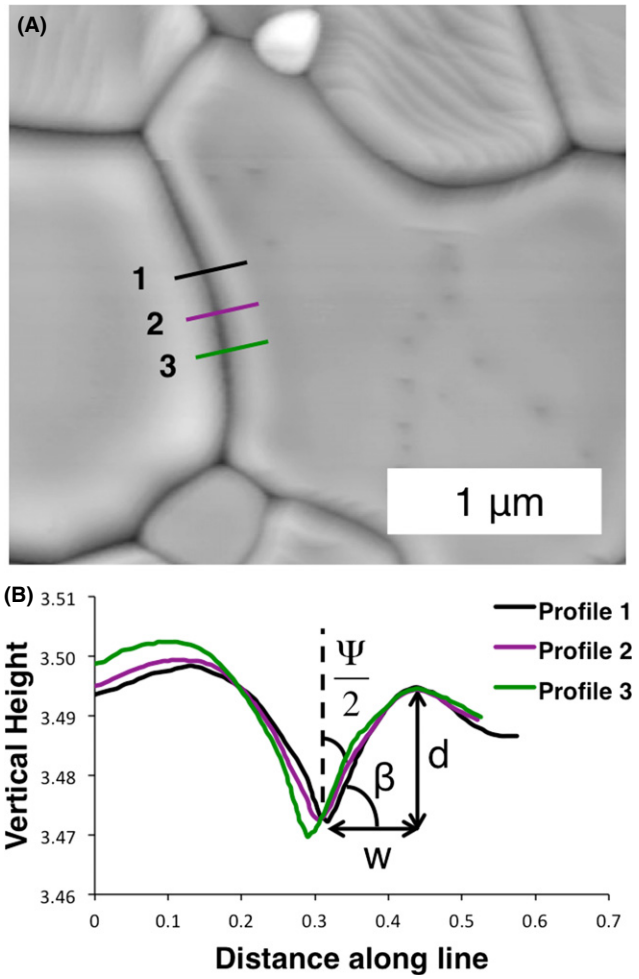

FIGURE 2 (A) Typical AFM image of a thermally grooved alumina surface. The lines indicate the positions from which the topographic traces in (B) were extracted. (B) Three groove profiles from which *W* and *d* are measured [Color figure can be viewed at wileyonlinelibrary.com]

to consider the finite size of the probe compared to the actual groove dimensions. Consideration of these factors has led to the conclusion that if the grooves are wide enough (W>1 μm), the finite probe size should not affect the measurement.[15] The corrections for smaller grooves have been calculated and were applied to the present data. However, no grooves with width less than 250 nm were considered; this limited the extent of the low temperature data, where reduced diffusivity means that it takes much longer to create wider grooves. It should also be noted that the value of m deviates from its ideal value of 4.73 as W/d becomes smaller. However, the relationship between m and W/d is known[17] and a correction was applied to account for this.

Finally, there are a number of approximations in Equation (1) that should be recognized when applying it to measurements. First, it is assumed that the two surface energies on either side of the groove root are the same and this is, in general, not true. Second, it is assumed that the grain boundary is normal to the surface plane and, again, this is not true in general. Third, it is assumed that the differentials of the surface and grain-boundary energy with respect to orientation are small enough to be ignored and this is, again, not true. Because of these approximations, the measurement of a single grain-boundary groove has little meaning. Therefore, our approach is to measure many grooves and examine the distribution of values of γ_{gb}/γ_s, which samples variations in the unknown parameters listed above. It has been shown that if enough thermal grooves are measured, the mean value and width of the distribution are reproducible characteristics of the sample;[17] here, we will take the mean value of γ_{gb}/γ_s as the quantity of interest and will refer to it as the relative grain-boundary energy.

The number of measurements at each temperature varied between 48 and 311 (see Table S1). To estimate the uncertainty of the mean value for each distribution, we tested its sensitivity to the number of measurements included in the calculation. Specifically, the mean value of γ_{gb}/γ_s was calculated using randomly selected subsets of the measurements. This process was repeated 10 times and an example of this analysis is illustrated in Figure S1. The standard deviation of the mean values calculated using 10 random samples, each containing 50% of the data, was taken to be the uncertainty of the mean value of γ_{gb}/γ_s calculated from all of the data.

3 | RESULTS

AFM images of the microstructures of the 100 ppm Y-doped alumina samples at temperatures between 1350°C and 1650°C are illustrated in Figure 3. All images are shown with the same field of view to emphasize the changes in the grain size. It should be noted that none of the AFM images showed any evidence for the precipitation of yttrium aluminum garnet (YAG). X-ray diffraction and mapping by energy-dispersive spectroscopy (EDS) also revealed no evidence for YAG precipitation. At the conclusion of the thermal treatments, the 100 ppm sample was fractured; the fracture was almost completely intergranular. Inspection by high-resolution SEM, coupled with EDS mapping, yielded no evidence for the precipitation of YAG. Therefore, we conclude that the added Y remained in solution or segregated to the boundaries during this experiment. We note that studies of the solubility of Y in alumina in this temperature range cover a wide range,[18–27] from less than 10 ppm[19] up to 200 ppm Y.[18]

AFM images of the microstructures of the 500 ppm Y-doped alumina samples at temperature between 1350°C and 1650°C are illustrated in Figure 4. At 1450°C, there is clear evidence for the precipitation of YAG. Note that this

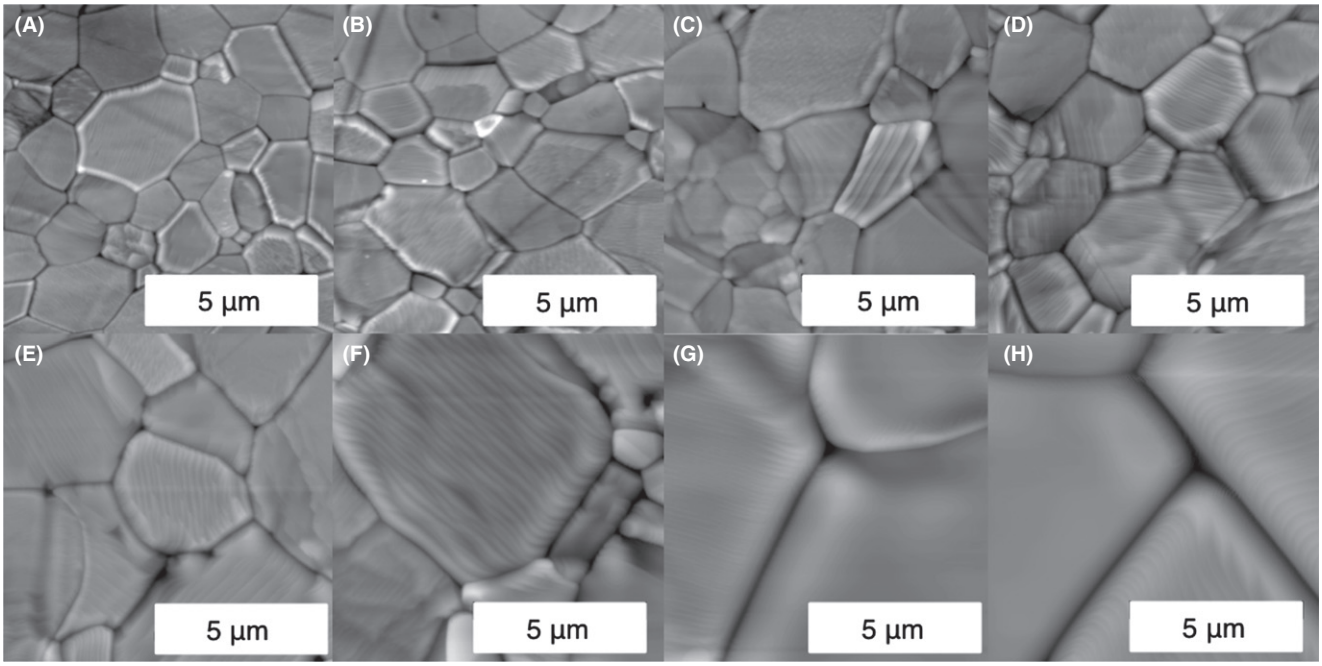

FIGURE 3 Representative AFM images of the 100 ppm Y-doped sample after grooving at (A) 1350°C (B) 1400°C (C) 1450°C (D) 1500°C (E) 1525°C (F) 1550°C (G) 1600°C (H) 1650°C

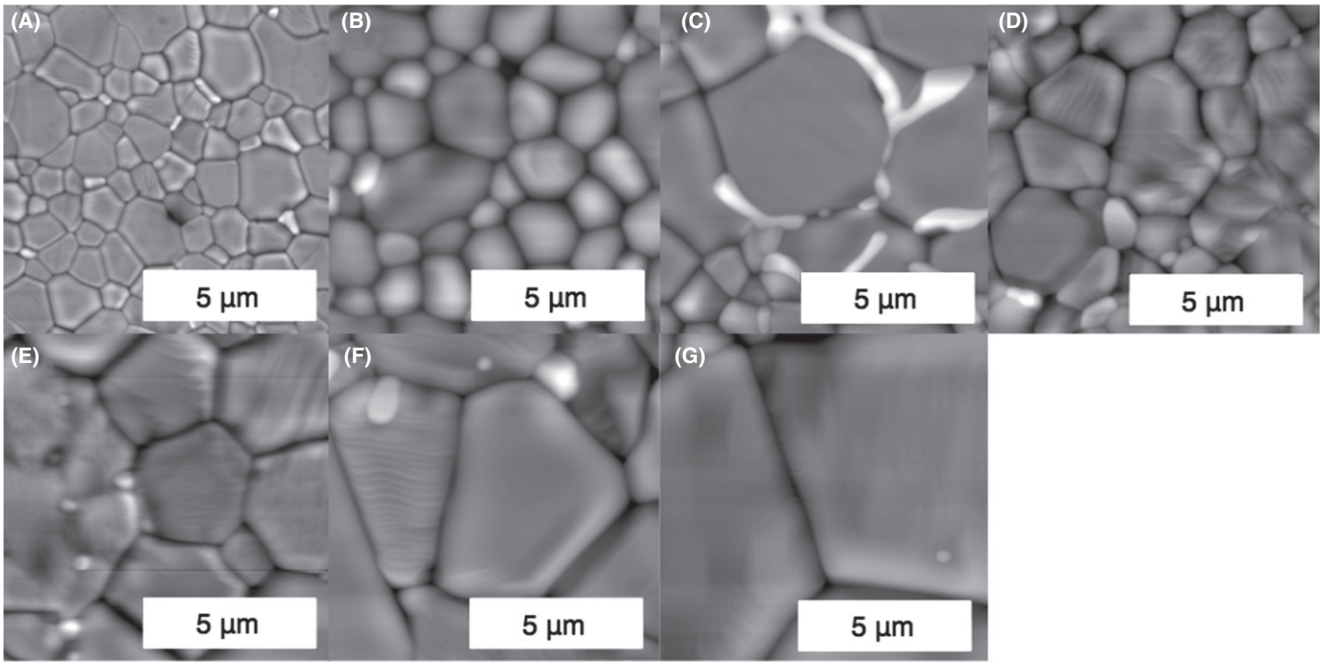

FIGURE 4 Representative AFM images of the 500 ppm Y-doped sample after grooving at (A) 1350°C (B) 1400°C (C) 1450°C (D) 1500°C (E) 1550°C (F) 1600°C (G) 1650°C

image was selected for the large, obvious precipitates, which are not typical of the entire surface. Based on its EBSD pattern, the structure of this precipitate is consistent with YAG and based on EDS, its composition is consistent with YAG. These data are included in the supplemental information (see Figure S2). At higher temperatures, the grain size increases significantly (also see Table 1).

The images in Figures 3 and 4 are only small areas of the samples. For each sample, large areas were imaged so that many grain-boundary thermal groove profiles could be measured. Figure 5 shows a cumulative distribution plot for all of the thermal grooves from samples annealed at 1550°C. If we consider the median value of the relative grain-boundary energy (a cumulative fraction of 0.5), then

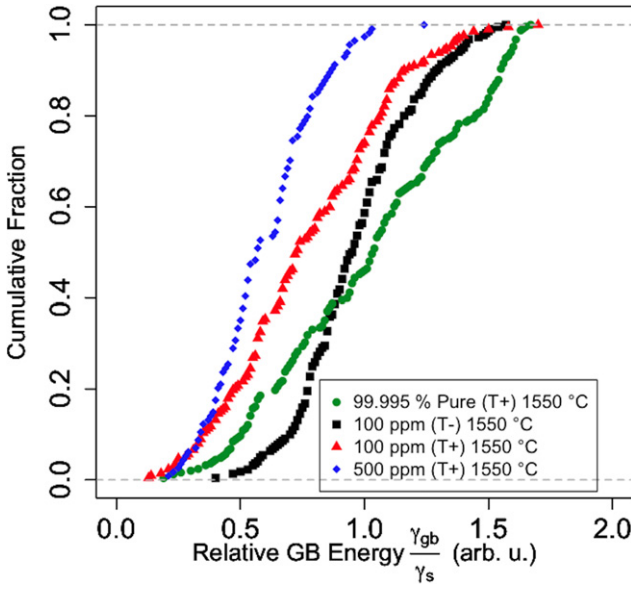

FIGURE 5 Cumulative distributions of relative grain-boundary energies for the samples at 1550°C [Color figure can be viewed at wileyonlinelibrary.com]

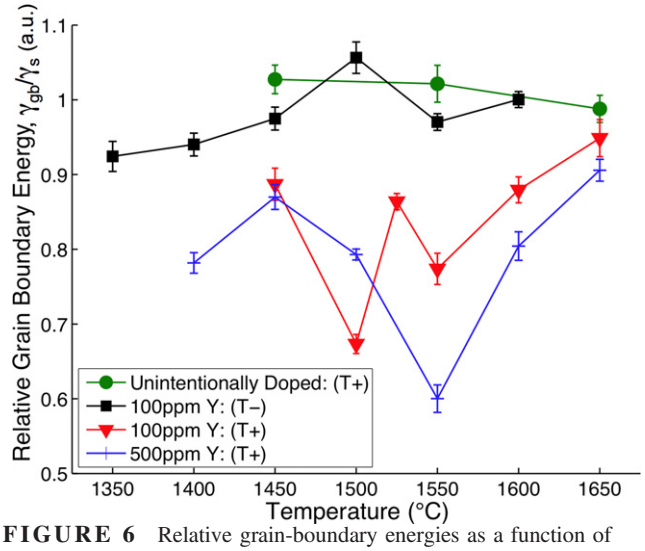

FIGURE 6 Relative grain-boundary energies as a function of temperature [Color figure can be viewed at wileyonlinelibrary.com]

the sample with the highest concentration of dopants (500 ppm Y-doped alumina) has the lowest relative grain-boundary energy and the 99.995% pure sample has the highest median energy, as one would expect from the influence of impurities on grain-boundary energies. Note that the median energies for the 100 ppm Y-doped samples (during heating and cooling) are between these two limits. Recall that YAG precipitated in the 500 ppm sample at a lower temperature, indicating that the grain boundaries in this sample are saturated with Y, in equilibrium with the YAG precipitates. Because the relative grain-boundary energies of this saturated specimen are lower than in the 100 ppm doped sample, it can be surmised that the Y content in the grain boundaries is also greater. This supports the idea that the Y content of the 100 ppm sample did not exceed the solubility limit of Y in alumina at 1550°C. When the different shapes of the distributions are compared, it appears the main effect of the dopants is to reduce the energy difference between the highest and lowest energy boundaries.

The mean relative grain-boundary energies for all of the samples are summarized in Figure 6. Note that for some of the samples, data collected at 1350°C and 1400°C is not included. In cases where the majority of the grooves were not wider than 250 nm, the distribution was deemed unreliable because of the convolution between the AFM tip and the groove shape, and these points are excluded.

Thermal grooves were measured in the 99.995% pure sample at 1450°C, 1550°C, and 1650°C. Over this range of temperature, the mean values decrease slightly, consistent with the effect of entropy on the grain-boundary free energy of a pure material. However, note that differences between these values are not greater than the estimated uncertainty. The mean values, which are close to 1.0, are similar to previous measurements. At 1600°C, Handwerker et al.[28] and Saylor et al.[15] both measured γ_{gb}/γ_s=1.2; at 1400°C, Dillon et al.[7] report a value of 1.11.

The grain boundary to surface energy ratio of the 500 ppm Y-doped sample varies significantly with temperature. The increase in energy from 1400°C to 1450°C is likely the result of the depletion of Y from the grain boundaries. Note that YAG precipitates were first observed at 1450°C and the precipitation reaction is expected to deplete excess solute from the boundaries, assuming they were initially supersaturated. Between 1450°C and 1550°C, there is a significant (30%) decrease in γ_{gb}/γ_s. This is consistent with the previously detected complexion transition.[7,13,29,30] The change occurs over a 100°C temperature range. This is consistent with the observation that not all grain boundaries transition at the same temperature. It has previously been demonstrated that higher (lower) energy grain boundaries undergo complexion transitions at lower (higher) temperatures.[13] Finally, after the minimum grain-boundary energy is reached at 1550°C, there is a significant increase in the relative grain-boundary energy. This is likely the result of the increasing bulk solubility of Y in alumina that depletes the grain boundaries.

The grain boundary to surface energy ratio of the 100 ppm Y-doped sample also decreases above 1450°C. It then increases toward 1650°C, where the relative energy is slightly greater than that of the 500 ppm doped sample. The points at 1525°C and 1550°C have an unexpected trend. It is possible that there is a second boundary transition at 1550°C that caused the decrease in energy. Between 1550°C and 1650°C, the energy undergoes an increase in energy similar to the 500 ppm sample. For both samples,

the relative grain-boundary energy is greater at the highest temperature than at the lowest temperature, which is most likely because of depletion of Y from the boundaries.

After the heat treatment at 1650°C, the measurements on the 100 ppm Y-doped sample were repeated at successively lower temperatures. The overall trend is that there is a decrease in the relative grain-boundary energy as the temperature is reduced, except for the increase that occurs at 1500°C. The overall decrease is consistent with the increasing segregation of solute to the boundaries at lower temperature. The increase in energy at 1500°C is consistent with a reversal of the transition that reduced the energy during heating, suggesting that the complexion transition is reversible. The absolute values of the energy are, on the other hand, quite different. It must be noted that the sample that is cooled in this experiment has a very different microstructure with respect to grain size and grain-boundary character distribution than the one that was heated and this may explain the difference. We will elaborate on this point in the next section.

4 | DISCUSSION

The temperature dependence of the relative grain-boundary energy of 99.995% pure alumina is consistent with expectations. The small decrease with increasing temperature is likely the result of the increasing importance of the entropic term in the free energy. More importantly, this sample serves as a "control", so that we can separate intrinsic properties of alumina grain boundaries from extrinsic solute-related effects in the Y-doped samples. The data from the 99.995% pure sample shows that the measurements can be made consistently within a range of ±0.05 arbitrary units and that changes in the grain-boundary free energy from entropy are similar to this value. Therefore, the much larger changes in the relative grain-boundary energy found in the other samples can be attributed to the interaction of the solute with the boundary.

The data from the Y-doped samples are consistent with the overall trend that as the temperature is increased, the solute is depleted from the grain boundary and the energy increases. However, there are also significant decreases in the relative grain-boundary energy in the temperature range from 1450°C and 1550°C. The temperature range corresponds to the point where abnormal grain growth begins. In other words, when there is a significant decrease in grain-boundary energy, some of the grain boundaries have much higher velocities. This higher grain-boundary velocity is indicated by some grains being significantly larger than others in the AFM images of samples heated in the 1450°C to 1550°C temperature range. It should be noted that, by itself, a lower grain-boundary energy reduces the driving force for grain growth and boundaries should, on average, have lower velocities. Therefore, the increased grain-boundary velocity with reduced grain-boundary energy suggests that the grain-boundary mobility must increase significantly. This transition in energy and mobility has previously been associated with a grain-boundary complexion transition[7,13] and that appears to be the best explanation for onset of abnormal grain growth at this temperature.[26,27,29]

The precipitation of YAG was only detected in the 500 ppm sample. As mentioned in the introduction, precipitation is expected to reduce the concentration of solute in the boundary and increase the relative grain-boundary energy. As expected, when YAG precipitates in the range between 1400°C and 1450°C, the relative grain-boundary energy increases by about 13%. It is not clear if the increase is from desegregation alone or if the boundaries were supersaturated at 1400°C and part of the increase is from reducing the boundary excess back to the saturated concentration.[11]

It should be noted that there are contradictory results in the literature on the solubility of Y in alumina. In this temperature range, it has been reported to be as low as 9 ppm[19] and as high as 200 ppm.[18] The available data in the literature is summarized in Figure S3. It is likely that at least part of the differences might be explained by the microstructural effect on the apparent solubility. At any temperature, there is clearly a single equilibrium value for the solubility of Y in a single crystal of alumina. We will refer to this as the intrinsic solubility. However, in a polycrystalline ceramic, excess solute can be accommodated at the grain-boundary. Because the amount of excess solute within the ceramic depends on the ratio of the grain-boundary area to the sample volume, we refer to this as the extrinsic solubility. The total apparent solubility in a ceramic (the amount of solute that can be added before a second phase occurs) is then the sum of the intrinsic and extrinsic solubilities and it will vary with grain size.

To make a quantitative estimate of how the extrinsic solubility (C_{ex}) varies with the grain diameter, D, we define it in the following way:

$$C_{ex} = \frac{\frac{1}{2}\Gamma A}{F_{Al} V} \tag{2}$$

where Γ is the grain-boundary excess of Y in alumina, in Y atoms per area, A is the grain-boundary area of a grain with diameter D, V is the grain volume, F_{Al} is the number of Al atoms per volume, and the factor of ½ accounts for the fact that each grain-boundary is shared between two grains. If we assume cube-shaped grains, $A=6D^2$ and $V=D^3$. Based on crystallographic data for alumina, $F_{Al}=47$ Al/nm^3. This leads to:

$$C_{ex} = \frac{0.064\Gamma}{D} \tag{3}$$

According to Gülgün et al.,[11] a typical value for Γ at saturation is 5 Y/nm^2. Therefore, at a grain size of 1 μm,

the extrinsic solubility can be as high as 300 ppm. By the time a grain size of 10 μm is reached, the excess solubility falls to about 30 ppm. For the 100 ppm Y sample, this implies an intrinsic solubility of at least 70 ppm, which is within the range of values reported previously.[18,19] Note that while the assumption of grain shape will affect the exact values, it will not change the order of magnitude. Considering that these are typical grain sizes in alumina ceramics, this may explain the wide range apparent solubilities that have been reported. It should be noted that there can also be another component to the extrinsic solubility associated with co-doping and this might also affect the apparent solubility.

Another factor that should not be ignored in the consideration of the data is the change in the types of grain boundaries in the samples as a function of temperature. In general, the populations of different grain-boundary types are inversely correlated with the grain-boundary energy[31,32] and they depend on the type and concentration of segregating impurities.[33] Because of this, when Y-doped alumina goes through the complexion transition, there is a change in the grain-boundary character distribution that reflects a change in the grain-boundary energy anisotropy.[29] This new grain-boundary character distribution is frozen in at high temperature, so the grain-boundary distribution in the 100 ppm Y-doped sample is different from the distribution that existed on heating. This might partially account for the differences between the heating and cooling curves in Figure 6. Note that the relative grain-boundary energy for the 100 ppm Y-doped sample after cooling to the lowest temperature is consistent, within experimental uncertainty, with the energy at the lowest temperature that could be measured in the sample before heating. The constancy of energy for a material with a different grain-boundary character distribution and grain size is likely the result of an interplay between changes in the grain boundary excess, the specific grain-boundary types, and how the excess affects the energies of those boundaries. Although we observe only an average result, the relationship between grain-boundary excess and the grain-boundary energy is likely to be different for each boundary.

The temperature dependence of the relative grain-boundary energy of the 100 ppm Y-doped sample indicated that both the segregation of Y to the boundaries on cooling is reversible and that the complexion transition is reversible. Overall, there is a decrease in the relative grain-boundary energy from 1600°C to 1350°C that could be explained by the segregation of Y from the grains to the grain boundary as the intrinsic solubility decreases with temperature. However, at 1500°C, there is an increase in relative energy. This is at the same temperature as the complexion transition that decreases the energy upon heating. Because the change in energy is more than our estimated uncertainty, we can conclude that this is the reverse of the complexion transition that occurs on heating and leads to an increase in the grain-boundary energy. Note that the reversibility of a surface complexion transition has been reported previously,[34] but this is the first indication that a grain-boundary complexion transition is also reversible. The reversibility of these transitions suggests that it will be possible to define processing routes that exploit the mobility differences in different complexions to control the microstructure.[30]

5 | CONCLUSION

Changes in the relative grain-boundary energy of Y-doped alumina, detected by the measurement of grain-boundary thermal grooves, likely result from the redistribution of solute from the grain boundaries to the bulk during heating and the reverse during cooling. The relative grain-boundary energy of a 99.995% pure sample decreases slightly with increasing temperature. However, there are larger changes in the measured energies for the 100 ppm and 500 ppm Y-doped samples during heating and cooling. Overall, the grain-boundary energies in the Y-doped samples increased with increasing temperature and (in the case of the 100 ppm Y-doped material) decreased with decreasing temperature. This is explained by Y at the boundaries dissolving in the bulk during heating, and resegregating to the boundaries during cooling. There are also abrupt reductions in the relative grain-boundary energy between 1450°C and 1550°C during heating that are associated with a complexion transition that increases grain-boundary mobility and leads to abnormal grain growth. For the 100 ppm Y-doped sample, there is a corresponding increase in the relative energy at this temperature when the sample is cooled, suggesting that the grain-boundary complexion transition is reversible.

ACKNOWLEDGMENT

The authors acknowledge support from the ONR-MURI program (grant no. N00014-11-0678). The authors also acknowledge use of the Materials Characterization Facility at Carnegie Mellon University supported by grant MCF-677785.

REFERENCES

1. Gupta D. Diffusion, solute segregations and interfacial energies in some material: an overview. *Interface Sci*. 2003;11:7–20.
2. Foiles SM. Temperature dependence of grain boundary free energy and elastic constants. *Scripta Mater*. 2010;62:231–234.
3. Najafabadi R, Srolovitz DJ, Lesar R. Thermodynamic and structural properties of [001] twist boundaries in gold. *J Mater Res*. 1991;6:999–1011.

4. Rheinheimer W, Bäurer M, Chien H, Rohrer GS, Handwerker CA, Blendell JE, Hoffmann MJ. The equilibrium crystal shape of strontium titanate and its relationship to the grain boundary plane distribution. *Acta Mater*. 2015;82:32–40.
5. Rheinheimer W, Hoffmann MJ. Non-Arrhenius behavior of grain growth in strontium titanate: new evidence for a structural transition of grain boundaries. *Scripta Mater*. 2015;101:68–71.
6. Dillon SJ, Harmer MP. Demystifying the role of sintering additives with "complexion". *J Eur Ceram Soc*. 2008;28:1485–1493.
7. Dillon SJ, Harmer MP, Rohrer GS. The relative energies of normally and abnormally growing grain boundaries in alumina displaying different complexions. *J Am Ceram Soc*. 2010;93:1796–1802.
8. Atkinson A, Taylor RI. The diffusion of Ni-63 along grain boundaries in nickel oxide. *Philos Magaz A-Phys Condens Matter Struct Defects Mech Prop*. 1981;43:979–998.
9. Barreau G, Brunel G, Cizeron G, Lacombe P. Diffusion in copper-silver system: heterodiffusion and chemical diffusion. Influence of low Cr, Te, Ti and Zr additions to copper. *Mem Sci Rev Met*. 1971;68:357–366.
10. Lange W, Hässner A, Mischer G. Messung der korngrenzendiffusion von Nickel-63 in nickel und gamma-eisen. *Phys Status Solidi*. 1964;5:63–71.
11. Gülgün MA, Voytovych R, Maclaren I, Rühle M, Cannon RM. Cation segregation in an oxide ceramic with low solubility: yttrium doped alpha-alumina. *Interface Sci*. 2002;10:99–110.
12. Cantwell PR, Tang M, Dillon SJ, Luo J, Rohrer GS, Harmer MP. Grain boundary complexions. *Acta Mater*. 2014;62:1–48.
13. Bojarski SA, Harmer MP, Rohrer GS. Influence of grain boundary energy on the nucleation of complexion transitions. *Scripta Mater*. 2014;88:1–4.
14. Bojarski SA, Ma S, Lenthe W, Harmer MP, Rohrer GS. Changes in the grain boundary character and energy distributions resulting from a complexion transition in Ca-doped yttria. *Metall Mater Transac A-Phys Metall Mater Sci*. 2012;43A:3532–3538.
15. Saylor DM, Rohrer GS. Measuring the influence of grain-boundary misorientation on thermal groove geometry in ceramic polycrystals. *J Am Ceram Soc*. 1999;82:1529–1536.
16. Mullins WW. Theory of thermal grooving. *J App Phys*. 1957;28:333–339.
17. Robertson WM. Grain-boundary grooving by surface diffusion for finite surface slopes. *J App Phys*. 1971;42:463–467.
18. Behera SK, Atomic structural features of dopant segregated grain boundary complexions in alumina by EXAFS, PhD Thesis. Bethlehem, Pennsylvania: Lehigh University;2010:1–223.
19. Cawley JD, Halloran JW. Dopant distribution in nominally yttrium-doped sapphire. *J Am Ceram Soc*. 1986;69:C195–C196.
20. Cho J, Chan HM, Harmer MP, Rickman JM. Influence of yttrium doping on grain misorientation in aluminum oxide. *J Am Ceram Soc*. 1998;81:3001–3004.
21. Cho J, Wang CM, Chan HM, Rickman JM, Harmer MP. Improved tensile creep properties of yttrium- and lanthanum-doped alumina: a solid solution effect. *J Mater Res*. 2001;16:425–429.
22. Cho J, Harmer MP, Chan HM, Rickman JM, Thompson AM. Effect of yttrium and lanthanum on the tensile creep behavior of aluminum oxide. *J Am Ceram Soc*. 1997;80:1013–1017.
23. Fang J, Thompson AM, Harmer MP, Chan HM. Effect of yttrium and lanthanum on the final-stage sintering behavior of ultrahigh-purity alumina. *J Am Ceram Soc*. 1997;80:2005–2012.
24. Koripella CR, Kröger FA. Electrical-conductivity of Al_2O_3-Fe+Y. *J Am Ceram Soc*. 1986;69(12):888–896.
25. Thompson AM, Soni KK, Chan HM, Harmer MP, Williams DB, Chabala JM, Levi-Setti R. Dopant distributions in rare-earth-doped alumina. *J Am Ceram Soc*. 1997;80:373–376.
26. Wang CM, Cargill GS, Chan HM, Harmer MP. X-ray absorption near-edge structure of grain-boundary-segregated Y and Zr in creep-resistant alumina. *J Am Ceram Soc*. 2002;85:2492–2498.
27. Wang CM, Cargill GS, Harmer MP, Chan HM, Cho J. Atomic structural environment of grain boundary segregated Y and Zr in creep resistant alumina from EXAFS. *Acta Mater*. 1999;47:3411–3422.
28. Handwerker CA, Dynys JM, Cannon RM, Coble RL. Dihedral angles in magnesia and alumina: distributions from surface thermal grooves. *J Am Ceram Soc*. 1990;73:1371–1377.
29. Bojarski SA, Stuer M, Zhao Z, Bowen P, Rohrer GS. Influence of Y and La additions on grain growth and the grain-boundary character distribution of alumina. *J Am Ceram Soc*. 2014;97:622–630.
30. Cantwell PR, Ma S, Bojarski SA, Rohrer GS, Harmer MP. Expanding time-temperature-transformation (TTT) diagrams to interfaces: a new approach for grain boundary engineering. *Acta Mater*. 2016;106:78–86.
31. Dillon SJ, Rohrer GS. Mechanism for the development of anisotropic grain boundary character distributions during normal grain growth. *Acta Mater*. 2009;57:1–7.
32. Rohrer GS. Grain boundary energy anisotropy: a review. *J Mater Sci*. 2011;46:5881–5895.
33. Papillon F, Rohrer GS, Wynblatt P. Effect of segregating impurities on the grain-boundary character distribution of magnesium oxide. *J Am Ceram Soc*. 2009;92:3044–3051.
34. Qian H, Luo J. Vanadia-based equilibrium-thickness amorphous films on anatase (101) surfaces. *Appl Phys Lett*. 2007;91:061909, 33pp.

SUPPORTING INFORMATION

Additional Supporting Information may be found online in the supporting information tab for this article.

How to cite this article: Kelly MN, Bojarski SA, Rohrer GS. The temperature dependence of the relative grain-boundary energy of yttria-doped alumina. *J Am Ceram Soc*. 2017;100:783–791.

Supplemental Information for:

The Temperature Dependence of the Relative Grain Boundary Energy of Yttria-doped Alumina

Madeleine N. Kelly, Stephanie A. Bojarski, and Gregory S. Rohrer

[1]Department of Materials Science and Engineering, Carnegie Mellon University, Pittsburgh, Pennsylvania 15213, USA

Table S1. Number of grain boundaries measured for each concentration and temperature plotted in Figure 6. (T+) denotes measurements made while increasing the temperature and (T-) denotes measurements made while decreasing the temperature

Concentration	Temperature (°C)	Number of boundaries
Unintentionally doped	1450	311
	1500	124
	1550	99
500 ppm	1400	65
	1450	109
	1500	172
	1550	57
	1600	48
	1650	99
100 ppm (T+)	1450	107
	1500	209
	1525	278
	1550	106
	1600	96
	1650	74
100 ppm (T-)	1350	82
	1400	136
	1450	120
	1500	95
	1550	110
	1600	76

Estimation of uncertainties in the relative grain boundary energy

Each point on the relative grain boundary energy versus temperature plot (Figure 6) is the mean of a distribution of grain boundary energies. To estimate the uncertainty, we

randomly selected different numbers of observations from complete sets of data and computed the means. As an example, Fig. S1 shows the mean value of the relative energy of 100 ppm Y-doped alumina sample heated at 1500 °C as a function of the number of observations, for randomly selected subsets. This was repeated 10 times. By comparing these curves, it is clear that when the mean relative energy is calculated from at least 30 % of the data, the results falls into a relatively constant band. Based on this, we used the standard deviation of the mean value of ten randomly selected subsets containing 50 % of the data as a measure of uncertainty. In this case, the 10 mean values of 105 randomly selected boundaries are (0.6887, 0.6681, 0.6617, 0.7123, 0.7013, 0.6545, 0.6810, 0.6659, 0.7173, 0.6611) and the standard deviation is 0.02.

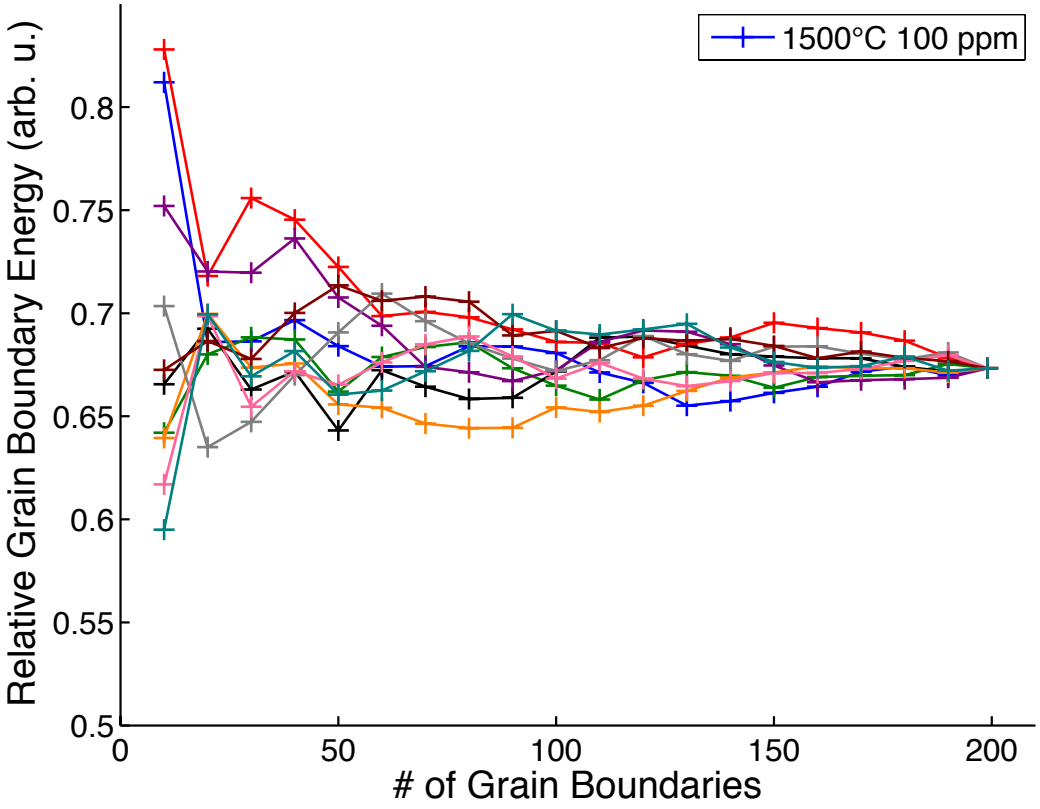

Figure S1. Mean values of 1500°C 100 ppm Y doped Alumina are plotted in 20 boundary increments, for the dataset randomized 10 times. Each colored curve is a different randomization of the same 100 ppm 1500°C dataset.

Evidence for YAG precipitation in the 500 ppm Y-doped alumina at heated at 1450 °C

The apparent second phase on the surface illustrated in Fig. 4(c) was examined by electron backscatter diffraction (EBSD) and energy dispersive spectroscopy (EDS). The green points in the EBSD phase identification map in Fig. S2(a) indexed as yttrium aluminum garnet and red points indexed as alumina. In the EDS map in Fig. S2(b), the red points represent aluminum, blue represent yttrium and green represents silicon. The combination of EBSD and EDS results indicated that a second phase of Si-rich YAG is present in the 500 ppm Y-doped alumina sample. The source of the Si contamination is not known, but it is a component of the furnace insulation and heating elements.

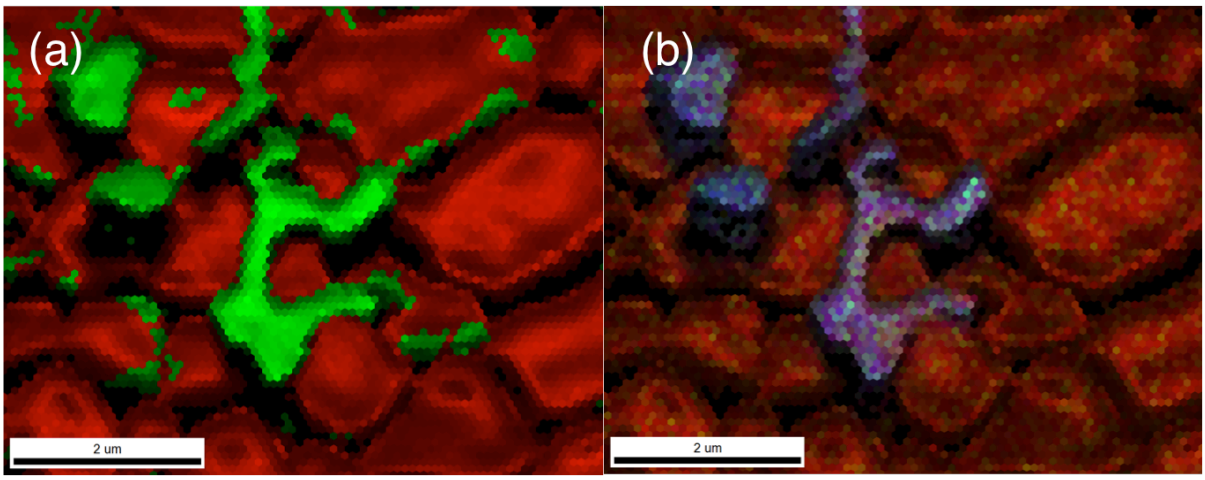

Figure S2. (a) EBSD map of YAG identified by green indexed points and alumina identified by red indexed points and (b) EDS map of elements aluminum (red), yttrium (blue) and silicon (green).

Summary of reported solubility and ranges of complexion stability in the Yttria-Alumina System

Publications that describe the microstructure of Y-doped alumina were reviewed and based on the reports of phase stability and abnormal grain growth, the phase diagram highlighting the ranges of stability for different complexions was developed (Fig. S3). The dashed solvus line between Al_2O_3 phase and Al_2O_3 + YAG phase is drawn based on reported values of the solubility limit as well as microstructural data (AGG observed). Points from studies where YAG precipitation is not mentioned are differentiated from those where it was specifically excluded. Complexion regions are also labeled as low temperature

complexion region, transition region and high temperature complexion region which was determined approximately by the onset of abnormal grain growth (beginning of transition region) and development to a more unimodal microstructure after AGG (beginning of High T Complexion Region). The solidus and liquidus lines are approximations.

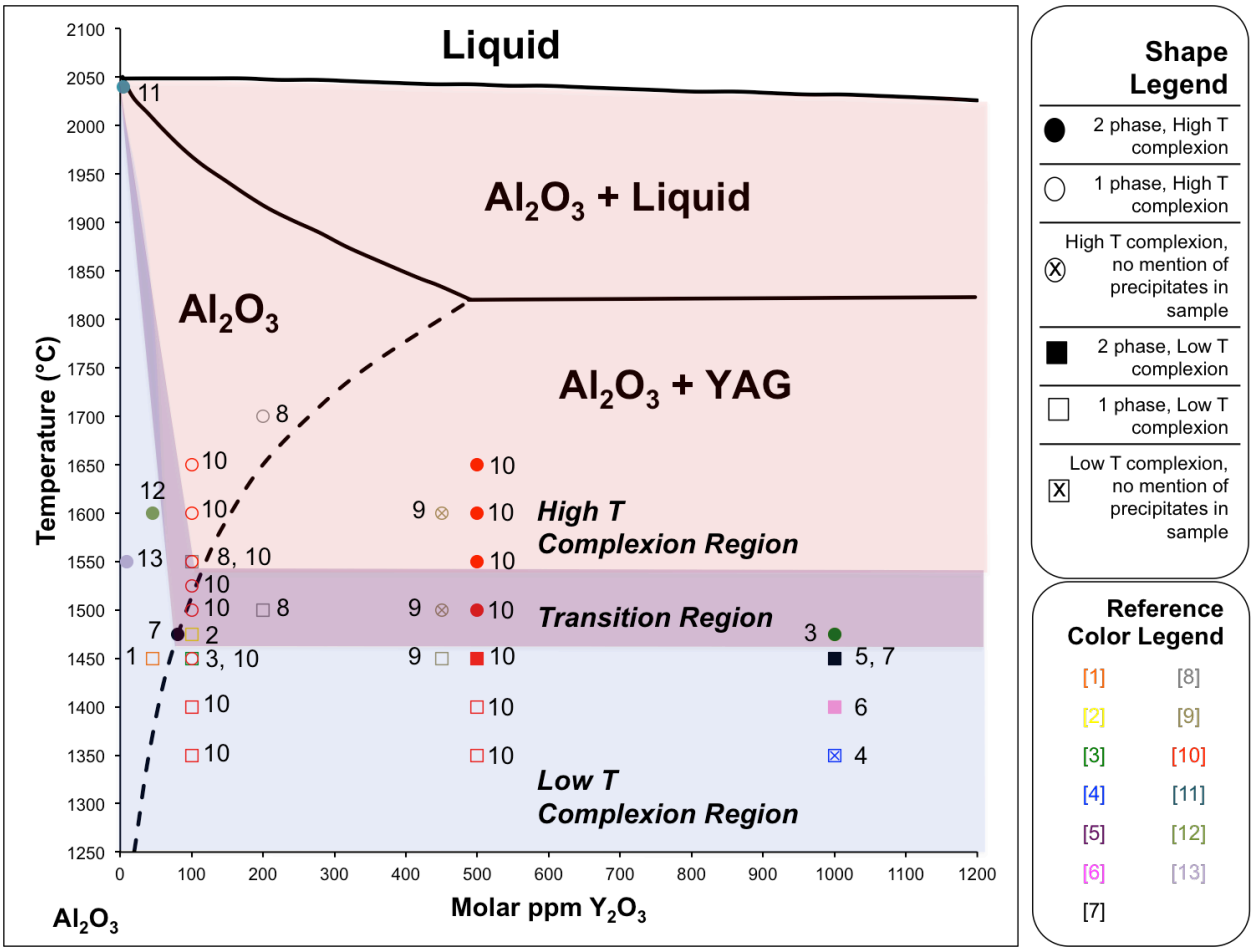

Figure S3. Yttria doped alumina phase diagram with overlaid complexion diagram. The current work is highlighted as reference [10].

References Cited

[1] J. Cho, C.M. Wang, H.M. Chan, J.M. Rickman, M.P. Harmer. "Improved tensile creep properties of yttrium- and lanthanum-doped alumina: a solid solution effect." *J Mater Res*, **16** [2] 425-429 (2001). http://dx.doi.org/10.1557/JMR.2001.0064

[2] C.M. Wang, G.S. Cargill III, H.M. Chan, M.P. Harmer. "X-ray Adsorption Near-Edge Structure of Grain-Boundary-Segregated Y and Zr in Creep-Resistant Alumina." *J Am Ceram Soc*, **85** [10] 2492-2498 (2002). DOI: 10.1111/j.1151-2916.2002.tb00486.x

[3] C.M. Wang, G.S. Cargill III, M.P. Harmer, H.M Chan, J. Cho "Atomic structural environment of grain boundary segregated Y and Zr in creep resistant alumina from EXAFS." *Acta Mater*, **47** [12] 3411-3422 (1999). doi:10.1016/S1359-6454(99)00210-4

[4] J. Fang, A.M. Thompson, M.P. Harmer, H.M. Chan. "Effect of Yttrium and Lanthanum on the Final-Stage Sintering Behavior of Ultrahigh-Purity Alumina." *J Am Ceram Soc*, **80** [8] 2005 2012 (1997). DOI: 10.1111/j.1151-2916.1997.tb03084.x

[5] J. Cho, M.P. Harmer, H.M. Chan, J.M. Rickman, A.M. Thompson. "Effect of Yttrium and Lanthanum on the Tensile Creep Behavior of Aluminum Oxide." *J Am Ceram Soc*, **80** [4] 1013-1017 (1997). DOI: 10.1111/j.1151-2916.1997.tb02936.x

[6] J. Cho, H.M. Chan, M.P. Harmer, J.M. Rickman. "Influence of Yttrium Doping on Grain Misorientation in Aluminum Oxide." *J Am Ceram Soc*, **81** [11] 3001-3004 (1998). DOI: 10.1111/j.1151-2916.1998.tb02726.x

[7] A.M. Thompson, K.K. Soni, H.M. Chan, M.P. Harmer, D.B. Williams, J.M. Chabala, R. Levi-Setti. "Dopant Distributions in Rare-Earth-Doped Alumina." *J Am Ceram Soc*, **80** [2] 373-376 (1997). DOI: 10.1111/j.1151-2916.1997.tb02840.x

[8] S.K Behera. "Atomic structural features of dopant segregated grain boundary complexions in alumina by EXAFS." *PhD dissertation, MSE, Lehigh*. 1-223 (2010). 3389944 http://gradworks.umi.com/33/89/3389944.html

[9] S.A. Bojarski, M. Stuer, Z. Zhao, P. Bowen, G. S. Rohrer. "Influence of Y and La Additions on Grain Growth and the Grain-Boundary Character Distribution of Alumina**."** *J. Am. Ceram. Soc.*, **97** [2] 622-630 (2014). DOI: 10.1111/jace.12669

[10] M. Kelly, S. Bojarski, G.S. Rohrer Thermal groove data (current work).

[11] J.D. Cawley, J.W. Halloran. "Dopant Distribution in Nominally Yttrium-Doped Sapphire." *J. Am. Ceram. Soc.*, **69** [8] Pages C-195–C-196 (1986). DOI: 10.1111/j.1151-2916.1986.tb04838.x

[12] C.R. Koripella, F.A. Kröger. "Electrical Conductivity of $A1_2O_3$: Fe + Y." J. Am. Ceram. Soc., **69** [12] 888-96 (1986). DOI: 10.1111/j.1151-2916.1986.tb07389.x

[13] M.A. Gülgün, R. Voytovych, I. Maclaren, M. Rühle. "Cation Segregation in an Oxide Ceramic with Low Solubility: Yttrium Doped α-Alumina." *Interface Science,* **10** [1] 99-110 (2002). DOI: 10.1023/A:1015268232315